Vector wave propagation method

M. Fertig[1,2,*] and K.-H. Brenner[1]

[1]*Chair of Opto-electronics, ZITI, University of Heidelberg, B6, 23-29, 68131 Mannheim, Germany*
[2]*IBM Research and Development, Microprocessor Development, Schoenaicher Strasse 220, 71032 Boeblingen, Germany*
**Corresponding author: matthias.fertig@ziti.uni-heidelberg.de*

Received December 14, 2009; revised January 27, 2010; accepted January 29, 2010; posted January 29, 2010 (Doc. ID 121400); published March 15, 2010

In this paper, we extend the scalar wave propagation method (WPM) to vector fields. The WPM [Appl. Opt. **32**, 4984 (1993)] was introduced in order to overcome the major limitations of the beam propagation method (BPM). With the WPM, the range of application can be extended from the simulation of waveguides to simulation of other optical elements like lenses, prisms and gratings. In that reference it was demonstrated that the wave propagation scheme provides valid results for propagation angles up to 85° and that it is not limited to small index variations in the axis of propagation. Here, we extend the WPM to three-dimensional vectorial fields (VWPMs) by considering the polarization dependent Fresnel coefficients for transmission in each propagation step. The continuity of the electric field is maintained in all three dimensions by an enhanced propagation vector and the transfer matrix. We verify the validity of the method by transmission through a prism and by comparison with the focal distribution from vectorial Debye theory. Furthermore, a two-dimensional grating is simulated and compared with the results from three-dimensional RCWA. Especially for 3D problems, the runtime of the VWPM exhibits special advantage over the RCWA.

OCIS codes: 200.0200, 240.0240, 250.0250.

1. INTRODUCTION

The scalar wave propagation method (WPM) [1]was introduced in order to overcome the major limitations of the beam propagation method (BPM). The latter has been primarily used for simulation of light propagation in waveguides. By application of a propagation operator derived from the slowly varying envelope approximation of the Helmholtz equation, propagation methods are typically restricted to forward propagation and the paraxial regime. In the original BPM scheme by Feit and Fleck [2], the propagation operator was split into two operators, a homogenous medium propagation in the averaged index and a thin element transmission through the index variation (i.e. the split step propagation scheme). Due to this operator splitting, the propagation is limited to paraxial propagation and small index variations in the axis of propagation. With the application of propagation methods to more general optical components, such as gradient index media, spheric and aspheric lenses, and gratings, there is much interest in removing some of these restrictions.

A higher-order propagation operator has been used by Hadley [3] to remove the paraxial limitation. Ma and van Keuren presented a three-dimensional wide-angle BPM in [4] for optical waveguide structures. A semivectorial wide angle BPM was presented by Lee and Vogoes in [5]. The BPM was extended to very wide angles in [6] but the error that depends on the separation of the propagation operator is still persistent in those methods. Several vector extensions of the BPM have been presented by Yamauchi *et al.* [7], Liu and Li [8], and Wanguemert-Perez and Molina-Fernandez [9]. Yamauchi *et al.* introduced a modified semivectorial beam propagation method retaining the longitudinal field component, Liu and Li analyzed the polarization modes of rib waveguides with a semivectorial BPM, and Wanguemert-Perez and Molina-Fernandez presented a fully-vectorial three-dimensional extension of the BPM. A third class of extensions is based on the finite element (FE) approach as published by Tsui *et al.* [10], Stern [11], Pinheiro *et al.* [12] and Obayya and Rahman [13]. The FE-based extensions of the BPM are optimized for scalar, semivectorial, and full-vectorial fields as well as numerically efficient methods in the order of citation. The fourth and last class of extensions in this brief overview of BPM-based methods is the multigrid approach that is used to reduce computational effort at regions in a system that allow a reduced degree of accuracy. Sewell *et al.* introduced a multigrid method for electromagnetic computation in [14]. Obviously. the BPM was subject to various optimizations, but except for the Padé approximation in [3] none of the BPM-based approaches overcomes the limitation that originates from the separation of the operators.

As noted above, the WPM was introduced by Brenner in 1993 [1] in order to overcome the paraxial limitation of the BPM. Instead of splitting the propagation operator into two parts, the WPM decomposes a field distribution into its plane wave components and performs a nonparaxial plane-wave propagation in an inhomogenous medium for each plane wave component. The field in the next step is then calculated as a sum over all propagated plane wave components. Since this sum cannot be performed in a fast Fourier transform (FFT) operation, the calculation time of the WPM grows with $\mathcal{O}(N^2)$, while the BPM calculation time, utilizing FFT and inverse FFT, is proportional to $\mathcal{O}(N\,log(N))$, taking N as the number of spatial samples. In [1], the accuracy of the (scalar) WPM was validated for propagation angles up to 85°. With the

wave propagation scheme, the range of applications can be significantly extended. It has been used for light propagation through gradient index and aspheric lenses and in a commercial software package [15]. Since the wave propagation scheme also extends the angular range into a domain where polarization effects become significant, a vectorial extension of the WPM is desirable. In this paper, we extend the WPM to three-dimensional vector fields by considering the polarization dependent Fresnel transmission coefficients. We verify the validity of this approach by transmission through a prism, by comparison with the focal distribution from vectorial Debye theory [17], and by grating diffraction.

Section 2 reiterates the limitations in the BPM from the separation of the operators. Section 3 introduces the definition of the input, and Section 4 briefly explains the ideas of the scalar WPM to introduce the vector extension and the nomenclature that is used in this paper. Section 5 describes the VWPM in detail, i.e. the theory for the vectorial extension of the WPM. Section 6 provides a vectorial extension of the BPM and covers various aspects of the numerical implementation of the VWPM. Section 7–9 verify the VWPM. The selected examples allow an easy theoretic and visual verification. The propagation of a Gaussian beam through a prism is verified by Snell's law and the Fresnel coefficients of amplitude. The vector components of a plane wave in the focus of an asphere are verified by vectorial Debye theory. The three-dimensional field distribution in a 2D grating is compared to the results from rigorous calculations using the 2D RCWA.

2. BEAM PROPAGATION METHOD

An analysis of the BPM serves to illustrate the differences introduced in the wave propagation scheme. The BPM uses a separation of the refractive index $n=\bar{n}+\delta n$. The separation of n provides the ability to calculate the propagation in a homogenous medium with averaged refractive index $\bar{n}$. The propagation is treated in the frequency domain by multiplication with the *diffraction operator* $\tilde{\mathcal{D}}$, which is equal to the *plane wave decomposition* (PWD) [18]. The separation of the refractive index introduces two sources of errors:

$$\begin{aligned}
&\sqrt{n^2k_0^2-(k_x^2+ky^2)}\\
&\quad=\sqrt{(\bar{n}+\delta n)^2k_0-(k_x^2+k_y^2)}=\sqrt{\bar{n}^2k_0^2-(k_x^2+ky^2)}\\
&\qquad\times\left(1+\frac{\bar{n}\,\delta n k_0^2}{\bar{n}^2k_0^2-(k_x^2+ky^2)}+\mathcal{O}(\delta n^2)\right)\\
&\quad\approx^{(1)}\sqrt{\bar{n}^2k_0^2-(k_x^2+ky^2)}+\frac{\bar{n}\,\delta n k_0^2}{\sqrt{\bar{n}^2k_0^2-(k_x^2+ky^2)}}\\
&\quad\approx^{(2)}\sqrt{\bar{n}^2k_0^2-(k_x^2+ky^2)}+k_0\delta n. \qquad (1)
\end{aligned}$$

A first error $\approx^{(1)}$ arises from the approximation of the square root by the linear part of its polynomial expansion to separate the term into two fractions that depend on $\bar{n}$ and δn. This error is in $\mathcal{O}(\delta n^2)$ and is responsible for the angle indiscriminate propagation through the index variation δn. A second error $\approx^{(2)}$ is caused by the paraxial approximation ($k_z^2\gg k_x^2+k_y^2$) that is necessary to separate the frequency dependency from the spatial dependency and to define the frequency dependent diffraction operator $\tilde{\mathcal{D}}$ and the space dependent phase shift operator $\mathcal{S}$ according to

$$\tilde{\mathcal{D}}(k_x,k_y)=e^{-i\delta z\sqrt{(\bar{n}k_0)^2-(k_x^2+k_y^2)}}, \qquad (2)$$

$$\mathcal{S}(x,y)=e^{-i\delta n(x,y)k_0\delta z}. \qquad (3)$$

Due to these approximations, the results are limited to paraxial propagation and small index variations in the axis of propagation.

3. DEFINITION OF THE INPUT SYSTEM

Let a system be defined by its z-discrete distribution of the complex refractive index $\hat{n}(x,y,z_j)=\hat{n}_j(x,y)\in\mathcal{C}$ (Eq. (4) below). The index j denotes the layer under investigation and N_z is the number of samples in the z-direction, i.e. the axis of propagation.

$$\hat{n}_j=n(x,y,z_j)+i\kappa(x,y,z_j). \qquad (4)$$

The aperture is defined by the XY-plane and has the physical dimensions $X=N_x\delta_x$ and $Y=N_y\delta_y$. The sampling is defined by δx, δy, and δz. An incident wave is supposed to propagate through the system $\mathcal{N}\in\mathcal{C}^{N_x\times N_y\times N_z}$.

4. SCALAR WAVE PROPAGATION METHOD

The WPM introduced in [1], like the BPM, decomposes the medium into slices of thickness δz. In each slice, the medium only depends on the lateral coordinates x and y. Unlike in the BPM, the propagation operator is not split into a spatial and frequency part. At the beginning of the propagation through each slice j, the incident scalar field u_j is decomposed into its plane wave components $\tilde{u}_j$ according to

$$\tilde{u}_j(\mathbf{k}_\perp)=\int\int u_j(\mathbf{r}_\perp)e^{-i\mathbf{k}_\perp\cdot\mathbf{r}_\perp}d^2\mathbf{r}_\perp, \qquad (5)$$

where the three-dimensional and the transversal positions and spatial frequencies are given by

$$\mathbf{r}=\begin{pmatrix}x\\y\\z\end{pmatrix},\quad \mathbf{r}_\perp=\begin{pmatrix}x\\y\end{pmatrix},\quad \mathbf{k}=\begin{pmatrix}k_x\\k_y\\k_z\end{pmatrix},\quad \mathbf{k}_\perp=\begin{pmatrix}k_x\\k_y\end{pmatrix}. \qquad (6)$$

The spatial frequencies are related to the wavenumber by $\mathbf{k}=2\pi\boldsymbol{\nu}$. The term *plane wave decomposition* (PWD) provides the central idea of the wave propagation scheme, because it emphasizes the decomposition of a scalar field $u(\mathbf{r})$ into its plane wave components $\tilde{u}(\mathbf{k})$ by the Fourier transformation. For each mode (i.e., Fourier coefficient), the contribution of the related transversal components of a plane wave is $w(\mathbf{k}_\perp,\mathbf{r}_\perp)=\tilde{u}(\mathbf{k}_\perp)\exp(i\mathbf{k}_\perp\cdot\mathbf{r}_\perp)$. The propagation through a layer j over a distance δz along the z-axis (i.e., the axis of propagation) of each plane wave component is then performed by the transmission

through an inhomogenous (i.e., a position- and frequency-dependent) phase element $\mathcal{P}_j(\mathbf{k}_\perp,\mathbf{r}_\perp)=\exp(i\delta z\sqrt{n_j^2(\mathbf{r}_\perp)k_0^2-\mathbf{k}_\perp^2})$, with $k_0=2\pi\nu_0=2\pi/\lambda_0$ and λ_0 the vacuum wavelength. Since the phase shift also depends on the local distribution of the refractive index $n(\mathbf{r}_\perp)$ a simple inverse Fourier transformation is not possible to calculate the propagated field. A summation (integration) of all deformed plane waves over the entire spectrum and aperture according to Eq. (7) below is necessary to obtain the propagated field at a distance δz. Unlike the BPM, the transmission through the locally varying refractive index $n_j(\mathbf{r}_\perp)$ depends on the angle of propagation (i.e., the spatial frequency) of each plane wave component. The propagated field in layer j at a distance $j\delta z$ is

$$u_j(\mathbf{r}_\perp)=\frac{1}{4\pi^2}\int\int w_{j-1}(\mathbf{k}_\perp,\mathbf{r}_\perp)\mathcal{P}_j(\mathbf{k}_\perp,\mathbf{r}_\perp)d^2\mathbf{k}_\perp. \tag{7}$$

This is the central equation of the wave propagation scheme. Note that for homogeneous media, Eq. (7) is equal to the PWD. Since the scheme is not limited to the paraxial regime, where vector effects usually can be ignored, the application to vectorial fields is reasonable.

5. VECTOR WAVE PROPAGATION METHOD

In the VWPM, we assume that a vector field $\mathbf{E}_{j-1}$ has traversed a layer $j-1$ of a systen $\mathcal{N}$. At the interface between layers $j-1$ and j the change in the refractive index introduces a boundary that requires a separation of the field into its TE- and TM-components. The vectorial field just before the interface between layer $j-1$ and j is decomposed into its Fourier components:

$$\tilde{\mathbf{E}}_{j-1}(\mathbf{k}_\perp)=\begin{pmatrix}\tilde{E}_{x,j-1}(\mathbf{k}_\perp)\\ \tilde{E}_{y,j-1}(\mathbf{k}_\perp)\\ \tilde{E}_{z,j-1}(\mathbf{k}_\perp)\end{pmatrix}=\int\int\mathbf{E}_{j-1}(\mathbf{r}_\perp)e^{i\mathbf{k}_\perp\cdot\mathbf{r}_\perp}d^2\mathbf{r}_\perp. \tag{8}$$

Each component $\mathbf{k}_\perp$ represents a plane wave $\mathbf{W}_{j-1}(\mathbf{r}_\perp,\mathbf{k}_\perp)=\tilde{\mathbf{E}}_{j-1}(\mathbf{k}_\perp)\exp(+i(\mathbf{k}_\perp\cdot\mathbf{r}_\perp+k_{z,j-1}z))$ with $k_{z,j-1}=\sqrt{(n_{j-1}(\mathbf{r}_\perp)k_0)^2-\mathbf{k}_\perp^2}$. As indicated by the plus in the exponent, it is important to take the positive solution from the square root and apply a positive propagation vector $\mathbf{k}$ in order to compute the field as described by the Fresnel and not the Lenserf theory.

A. Lateral Field Dependence

According to the Maxwell equation, in the absence of charges, $div(\mathbf{D})=0$, the x-, y-, and z-components of $\mathbf{W}_{j-1}(\mathbf{r}_\perp,\mathbf{k}_\perp)$ depend on each other. The z-component is related to the lateral components by solving

$$0=grad(\varepsilon(\mathbf{r}_\perp))\cdot\mathbf{W}(\mathbf{k}_\perp,\mathbf{r}_\perp)+\varepsilon(\mathbf{r}_\perp)div(\mathbf{W}_{j-1}(\mathbf{k}_\perp,\mathbf{r}_\perp)) \tag{9}$$

for each plane wave component. Using $div(\mathbf{W}_{j-1}(\mathbf{k}_\perp,\mathbf{r}_\perp))=i\mathbf{k}\cdot\mathbf{W}_{j-1}(\mathbf{k}_\perp,\mathbf{r}_\perp)$ we obtain

$$\tilde{E}_{z,j-1}=\frac{(i\varepsilon_{x,j-1}/\varepsilon-k_x)\tilde{E}_x+(i\varepsilon_{y,j-1}/\varepsilon-k_y)\tilde{E}_y}{k_{z,j-1}}=-\frac{k'_{x,j-1}\tilde{E}_x+k'_{y,j-1}\tilde{E}_y}{k_{z,j-1}}, \tag{10}$$

where $\varepsilon_{x,j-1}$ and $\varepsilon_{y,j-1}$ are the x- and y-components of the gradient of ε in layer $j-1$. The z-component of the gradient is zero, since we assume that $\varepsilon(\mathbf{r}_\perp)$ in each layer varies only in the lateral—not in the z-direction. With Eq. (10), it is sufficient in Eq. (8) to consider only the x- and y-components of the transform. We distinguish two- and three-dimensional vectors by $\mathbf{E}^{(2)}$ and $\mathbf{E}$.

B. Transfer at the Interface

As mentioned before, the transfer at the interface between layers $j-1$ and j requires a separation of the field into its TE- and TM-field components. Each component is then weighted by the Fresnel transmission coefficients, and the results are combined using the transmitted unit vectors of TE- and TM-polarization. The vectorial plane wave amplitude behind the interface can be expressed by

$$\tilde{\mathbf{E}}_j(\mathbf{k}_\perp)=t_{TE}\tilde{E}_{TE,j}\mathbf{e}_{TE}+t_{TM}\tilde{E}_{TM,j}\mathbf{e}_{TM,j}, \tag{11}$$

where the TE- and TM-field components are given by

$$\tilde{E}_{TE,j}(\mathbf{k}_\perp)=\tilde{\mathbf{E}}_j\cdot\mathbf{e}_{TE}, \tag{12}$$

$$\tilde{E}_{TM,j}(\mathbf{k}_\perp)=\tilde{\mathbf{E}}_{j-1}\cdot\mathbf{e}_{TM,j-1}, \tag{13}$$

and the unit vectors of TE- and TM-polarization before and behind the interface are given by

$$\mathbf{e}_{TE}=\mathbf{e}_{TE,j}=\mathbf{e}_{TE,j-1}=\frac{(\mathbf{e}_z\times\mathbf{k}_{j-1})}{|\mathbf{e}_z\times\mathbf{k}_{j-1}|}=\frac{1}{k_\perp}\begin{pmatrix}-k_y\\ k_x\\ 0\end{pmatrix} \tag{14}$$

and

$$\mathbf{e}_{TM,j-1}=\frac{(\mathbf{e}_{TE}\times\mathbf{k}_{j-1})}{|\mathbf{e}_{TE}\times\mathbf{k}_{j-1}|}=\frac{1}{n_{j-1}(\mathbf{r}_\perp)k_0k_\perp}\begin{pmatrix}k_xk_{z,j-1}\\ k_yk_{z,j-1}\\ -k_\perp^2\end{pmatrix}. \tag{15}$$

The unit vector of the TM-polarization behind the interface is given by

$$\mathbf{e}_{TM,j}=\frac{(\mathbf{e}_{TE}\times\mathbf{k}_j)}{|\mathbf{e}_{TE}\times\mathbf{k}_j|}. \tag{16}$$

The propagtion vectors $\mathbf{k}_{j-1}$ and $\mathbf{k}_j$ follow from the continuity of the lateral components $k_{x,j-1}=k_{x,j}$, $k_{y,j-1}=k_{y,j}$ and $k_{z,j-1}=\sqrt{(n_{j-1}k_0)^2-k_\perp^2}$, $k_{z,j}=\sqrt{(n_jk_0)^2-k_\perp^2}$. Note that $\mathbf{e}_{TM,j-1}$ as well as $\mathbf{e}_{TM,j}$ depend on the lateral position, since the index of refraction as well as the z-component of the

k-vectors are position dependent. Combining Eqs. (11) and (13), and Eqs. (14)–(16), we can express the transfer at the interface by the matrix operation

$$\tilde{\mathbf{E}}_j^{(2)}(\mathbf{k}_\perp,\mathbf{r}_\perp)=\mathbf{M}_j(\mathbf{k}_\perp,\mathbf{r}_\perp)\cdot\tilde{\mathbf{E}}_{j-1}^{(2)}(\mathbf{k}_\perp). \tag{17}$$

$\tilde{\mathbf{E}}_j^{(2)}$ is a transversal subvector of the electric field spectrum $\tilde{\mathbf{E}}_j$ behind the boundary. The matrix $\mathbf{M}_j(\mathbf{k}_\perp,\mathbf{r}_\perp)$ can be expressed as

$$\mathbf{M}_j(\mathbf{k}_\perp,\mathbf{r}_\perp)=\frac{1}{k_\perp^2}\begin{pmatrix} k_y^2 t_{TE}+k_x^2\hat{t}_{TM}(1-i\hat{\varepsilon}_{x,j-1}) & k_xk_y(\hat{t}_{TM}(1-i\hat{\varepsilon}_{y,j-1})-t_{TE}) \\ k_xk_y(\hat{t}_{TM}(1-i\hat{\varepsilon}_{x,j-1})-t_{TE}) & k_x^2 t_{TE}+k_y^2\hat{t}_{TM}(1-i\hat{\varepsilon}_{y,j-1}) \end{pmatrix} \tag{18}$$

with

$$\hat{\varepsilon}_{x,j-1}=f_j\frac{\varepsilon_{x,j-1}}{k_x},\quad \hat{\varepsilon}_{y,j-1}=f_{j-1}\frac{\varepsilon_{y,j-1}}{k_y},$$

$$f_{j-1}=\frac{k_\perp^2}{n_{j-1}^2k_{j-1}^2},\quad k_{j-1}=n_{j-1}k_0, \tag{19}$$

and

$$\hat{t}_{TM}=\frac{n_{j-1}k_{z,j}}{n_jk_{z,j-1}}t_{TM}. \tag{20}$$

The Fresnel coefficients for transmission are

$$t_{TE}=\frac{2k_{z,j-1}}{k_{z,j-1}+k_{z,j}},$$

$$t_{TM}=\frac{2n_{j-1}n_jk_{z,j-1}}{n_j^2k_{z,j-1}+n_{j-1}^2k_{z,j}}. \tag{21}$$

Using Eq. (20), the modified transmission coefficient for TM polarization can be simplified to

$$\hat{t}_{TM}=\frac{2n_{j-1}^2k_{z,j}}{n_j^2k_{z,j-1}+n_{j-1}^2k_{z,j}}. \tag{22}$$

C. Propagation Step

With Eq. (17), the two-dimensional field contribution behind the interface is known. To complete the propagation through one layer, we apply a propagation of the wave through the inhomogeneous medium with thickness δz. Considering the interface at $z=0$ at the beginning of each layer, a field component that propagated a distance δz is then

$$\mathbf{W}_j^{(2)}(\mathbf{k}_\perp,\mathbf{r}_\perp)=\tilde{\mathbf{E}}_j^{(2)}(\mathbf{k}_\perp)e^{+i(\mathbf{k}_\perp\cdot\mathbf{r}_\perp+k_{z,j}\delta z)}. \tag{23}$$

The propagated z-component is then calculated according to Eq.(10), from the space derivatives $\varepsilon_{j,x}$ and $\varepsilon_{j,y}$ of ε in layer j. The resulting field distribution at the end of layer j is obtained by a summation of all field components:

$$\mathbf{E}_j(\mathbf{r}_\perp)=\int\int\mathbf{W}_j(\mathbf{k}_\perp,\mathbf{r}_\perp)d^2\mathbf{k}_\perp. \tag{24}$$

D. Magnetic Vector and Poynting Vector

The electric vector $\mathbf{E}$ and magnetic vector $\mathbf{H}$ of a transversal electromagnetic wave are related by the transversality

$$\tilde{\mathbf{H}}=\sqrt{\frac{\varepsilon\varepsilon_0}{\mu\mu_0}}\left(\frac{\mathbf{k}}{k}\times\tilde{\mathbf{E}}\right). \tag{25}$$

Using Eq. (10), we apply Eq. (25) to the transversal components of the E-field and derive the magnetic vector in layer j from a matrix multiplication according to

$$\tilde{\mathbf{H}}_j=\mathbf{T}_j\cdot\tilde{\mathbf{E}}_j^{(2)} \tag{26}$$

with $\tilde{\mathbf{E}}_j^{(2)}$ as the x- and y-components of the three-dimensional spectrum $\tilde{\mathbf{E}}_j$ in layer j. $\mathbf{T}$ is derived from Eq. (25) as

$$\mathbf{T}_j(\boldsymbol{\nu}_\perp,\mathbf{r}_\perp)=\frac{1}{kk_{z,j}}\sqrt{\frac{\varepsilon\varepsilon_0}{\mu\mu_0}}\begin{pmatrix} -k'_{x,j}k_y & -(k_yk'_{y,j}+k_{z,j}^2) \\ k_xk'_{x,j}+k_{z,j}^2 & k_xk'_{y,j} \\ -k_yk_{z,j} & k_xk_{z,j} \end{pmatrix}. \tag{27}$$

The *Poynting vector* $\mathbf{S}$ is then derived from the magnetic field vector $\mathbf{H}_j(\mathbf{r}_\perp)=1/(2\pi)^2\int\int\tilde{\mathbf{H}}_j(\mathbf{k}_\perp,\mathbf{r}_\perp)e^{i2\pi\,\mathbf{k}_\perp\cdot\mathbf{r}_\perp}d^2\mathbf{k}_\perp$ by

$$\mathbf{S}=\frac{1}{2}Re(\mathbf{E}(\mathbf{r})\times\mathbf{H}^*(\mathbf{r})) \tag{28}$$

with $\mathbf{H}^*$ as the complex conjugate of $\mathbf{H}$. The energy flux through the boundaries is then the z-component of the Poynting vector.

6. ALGORITHM OF THE VWPM

A system $\mathcal{N}$ is split into N_z layers and sampled at N_x and N_y locations. The spatial frequencies $k_x=2\pi p\,\delta\nu_x=2\pi p/(N_x\delta x)$ and $k_y=2\pi q\,\delta\nu_y=2\pi q/(N_y\delta y)$ are determined by the sampling $(\delta x,\delta y)$ in the aperture. Each layer is orthogonal to the axis of propagation. A vector field is propagating through the system $\mathcal{N}$ layer by layer according to the VWPM equations that have been introduced in the previous section. Each layer j has a layer of incidence $j-1$ and a layer of propagation j. For the first iteration $j=0$, the incident layer is modeled by a homogeneous medium (i.e., $n_{extern}(x,y)=const$) or by a copy of layer 0. The incident wave is considered in front of the boundary of layer $j-1$ and j. The *first step* of the j-th iteration in the

z-axis is the plane wave decomposition of the field,

$$\mathbf{E}_{j-1}^{(2)}(m\,\delta x,n\,\delta y)=\begin{pmatrix}E_{x,j-1}\\E_{y,j-1}\end{pmatrix}\Rightarrow_{FFT}\begin{pmatrix}\tilde{E}_{x,j-1}\\\tilde{E}_{y,j-1}\end{pmatrix}=\tilde{\mathbf{E}}_{j-1}^{(2)}(p\,\delta k_x,q\,\delta k_y). \tag{29}$$

The *second step* applies the transformation matrix $\mathbf{M}$ for each spatial frequency $(p\,\delta k_x,q\,\delta k_y)$ and all locations $(m\,\delta x,n\,\delta y)$ in the aperture. The transmitted plane wave components for the electric field vector are derived from the spectrum according to

$$\begin{pmatrix}EX_j(p\,\delta k_x,q\,\delta k_y,m\,\delta x,n\,\delta y)\\EY_j(p\,\delta k_x,q\,\delta k_y,m\,\delta x,n\,\delta y)\end{pmatrix}:=\mathbf{M}_j\cdot\tilde{\mathbf{E}}_{j-1}^{(2)}. \tag{30}$$

The spatial derivatives $\varepsilon_{j,x}$ and $\varepsilon_{j,y}$ in $\mathbf{M}_j$ and $\mathbf{T}_j$ are derived from the symmetric average

$$\varepsilon_{j,x}(m\,\delta x,n\,\delta y)=\frac{n_j^2((m+1)\,\delta x,n\,\delta y)-n_j^2((m-1)\,\delta x,n\,\delta y)}{2\,\delta x},$$

$$\varepsilon_{j,y}(m\,\delta x,n\,\delta y)=\frac{n_j^2(m\,\delta x,(n+1)\,\delta y)-n_j^2(m\,\delta x,(n-1)\,\delta y)}{2\,\delta y}. \tag{31}$$

The propagated electric field $\tilde{\mathbf{W}}_j$ through the position- and frequency-dependent phase element is again described by Eq. (23). The propagated magnetic field vector of a spatial frequency is then derived from the x- and y-component of the electric field according to

$$\begin{pmatrix}HX_j(p\,\delta k_x,q\,\delta k_y,m\,\delta x,n\,\delta y)\\HY_j(p\,\delta k_x,q\,\delta k_y,m\,\delta x,n\,\delta y)\\HZ_j(p\,\delta k_x,q\,\delta k_y,m\,\delta x,n\,\delta y)\end{pmatrix}:=\mathbf{T}_j\cdot\begin{pmatrix}WX_j(p\,\delta k_x,q\,\delta k_y,m\,\delta x,n\,\delta y)\\WY_j(p\,\delta k_x,q\,\delta k_y,m\,\delta x,n\,\delta y)\end{pmatrix}. \tag{32}$$

The z-component WZ_j is obtained from Eq. (10) in layer j, and the three-dimensional electrical field vector $\mathbf{E}(m\,\delta x,n\,\delta y)$ and magnetic vector $\mathbf{H}(m\,\delta x,n\,\delta y)$ in the transmitted layer j are then obtained by the summation over each frequency:

$$\mathbf{E}_j(m\,\delta x,n\,\delta y):=\sum_p\sum_q\begin{pmatrix}WX_j\\WY_j\\WZ_j\end{pmatrix}. \tag{33}$$

A. VWPM in a Homogeneous Medium

In a homogeneous medium, the refractive index is constant and the propagation operator $\mathcal{P}$ is therefore space independent. For propagation through a homogeneous layer, the VWPM is hence equal to the vectorial version of the PWD:

$$\mathbf{E}_j=\mathcal{F}^{-1}\{\tilde{\mathbf{E}}_j e^{+ik_z\delta z}\}. \tag{34}$$

B. Vectorial BPM

In the vectorial BPM (VBPM), the propagation through a layer is split into two steps. In the first step, the propagation in the homogeneous medium is performed using the average refractive index $\bar{n}$ in the diffraction operator $\tilde{\mathcal{D}}(\mathbf{k}_\perp)$ [Eq. (2)]. This step is already described in Subsection 6.A. The second step adjusts the phase according to the spatial deviation of the refractive index $\delta n(\mathbf{r}_\perp)=n(\mathbf{r}_\perp)-\bar{n}$ by multiplication with $\mathcal{S}(\mathbf{r}_\perp)$ [Eq. (3)]. For the VBPM we extend the BPM by an additional step, the transfer of the vectorial wave at the interface. The electric field spectrum is multiplied with the transfer matrix $\mathbf{M}(\mathbf{k}_\perp)$ using a constant index $\bar{n}$. Thus, $\mathbf{E}_j(\mathbf{r})$ is then derived from $\mathbf{E}_{j-1}^{(2)}(\mathbf{r})$ according to

$$\mathbf{E}_j=\mathcal{S}_j\mathcal{F}^{-1}\{\mathbf{M}_j\cdot\mathcal{F}\{\mathbf{E}_{j-1}^{(2)}\}\tilde{\mathcal{D}}\}. \tag{35}$$

The z-component is calculated from Eq. (10) in the homogeneous medium prior to the inverse Fourier transformation.

7. TWO-DIMENSIONAL SIMULATION OF REFRACTION AT A PRISM

A 2D simulation of a Gaussian beam that propagates through a prism provides an easy and visual way to verify the VWPM. The results are compared to the results from theory, and then the increased accuracy of the VWPM is by a comparison with the results from the VBPM. The simulated locations of the propagated peak and the amplitude of the Gaussian beam are also verified against the results from theory. The refractive index of the prism is $n_P=2.5$ and the surrounding refractive index $n=1$. The back boundary of the prism has a slope of 20°. The aperture has a width of $X=200$ μm and the Gaussian beam propagates a distance of $Z=130$ μm. The number of samples in the aperture is $N_x=512$ and in the axis of propagation $N_z=333$. The thickness of the prism D is 72.8 μm and the propagation distance after the prism at $x=0$ is $p=73.6$ μm. d is then 20 μm. The incident Gaussian beam is TE-polarized with a peak amplitude of 1 V/m. The wavelength is 4 μm and the waist diameter is 40 μm. The beam passes the front boundary at vertical incidence in the center of the aperture. The left subplot of Fig. 1 shows the geometry of the prism and the design parameters of the scene. The right plot shows the amplitude $|\mathbf{E}|$ of the propagating Gaussian beam. Snell's law and the Fresnel coefficients from literature are applied to the two boundaries in the configuration in order to calculate the exact location (59.1 μm) and amplitude (0.936 V/m) of the Gaussian beam in the output aperture.

Figure 2 compares the amplitudes at $z=130$ μm, calculated with the VBPM (left) and VWPM (right). The dashed lines represent the exact results for amplitude (horizontal line) and position (vertical line). Obviously, the VBPM deviates in the position of the peak. The peak has its maximum at $x=45.21$ μm with an amplitude of 0.947 V/m. The amplitude simulated by the VWPM is shown in the right subplot of Fig. 2. The peak position shows a good match to Snell's theory at $x=59.375$ μm and the amplitude at $z=130$ is 0.928 V/m. The deviation of the position from the exact result in this case is in the range of the sampling. We assume the deviation in the amplitude to be caused by an increased beam divergence

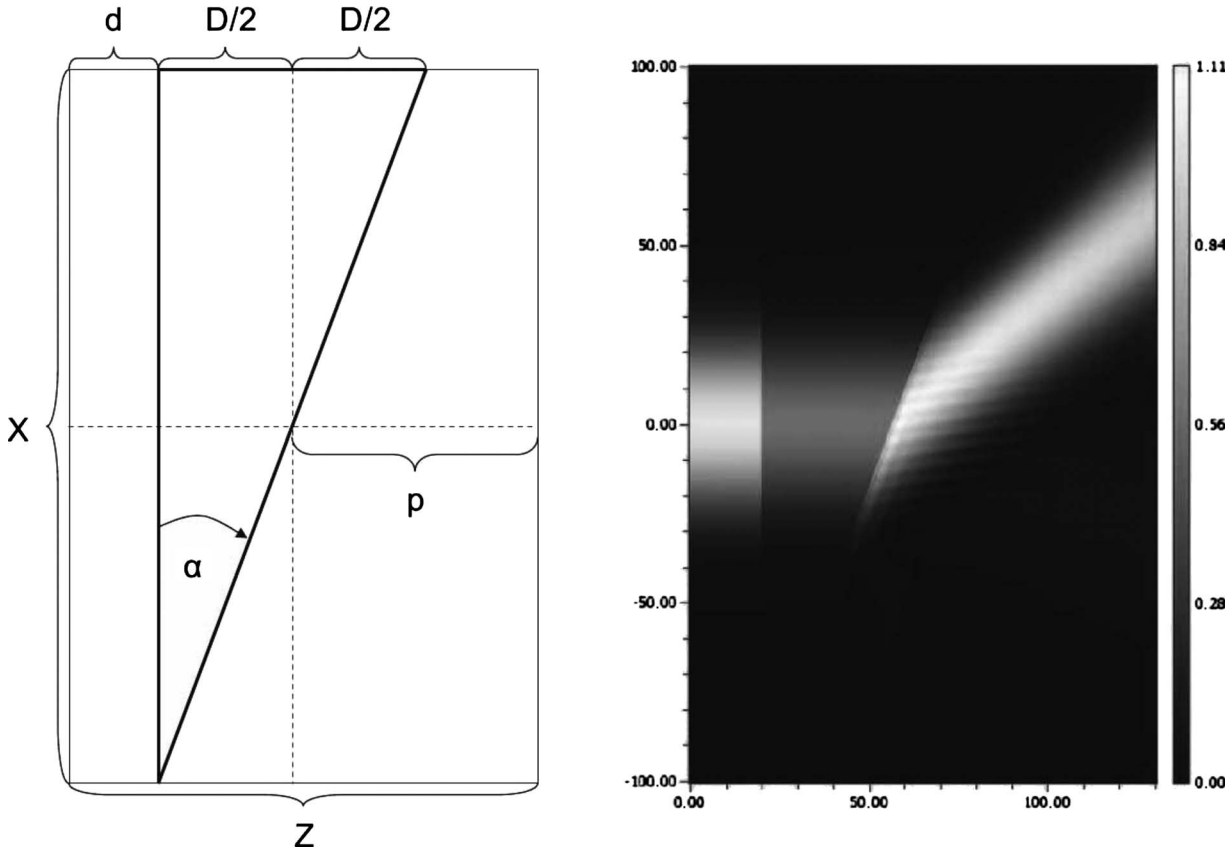

Fig. 1. 2D simulation of a prism. Left: Schematic description and design parameters. Right: Propagating Gaussian beam simulated with the VWPM.

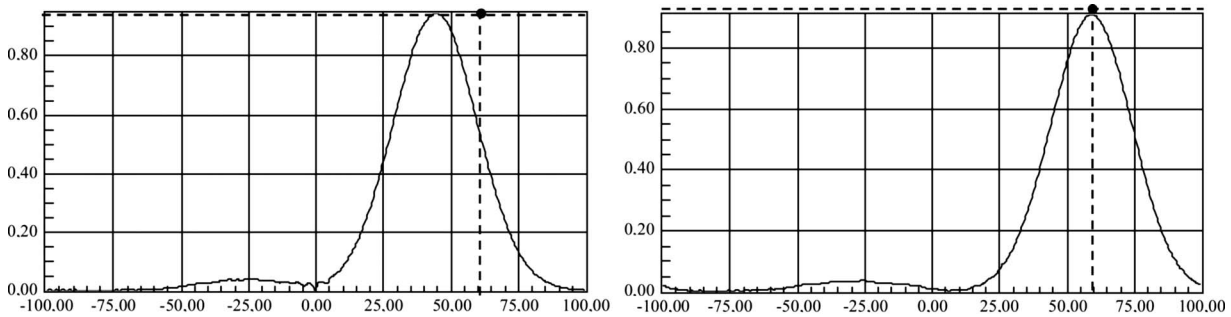

Fig. 2. Left: Propagated Gaussian beam with the VBPM. Right: Propagated Gaussian beam with the VWPM. The dashed lines show the exact result from theory.

that originates from the larger propagation distance at high refraction angles. No absorption has been considered in the entire scene.

8. THREE-DIMENSIONAL SIMULATION OF A PERFECT ASPHERE

To show the benefits of nonparaxial propagation, a three-dimensional asphere with a high numeric aperture is simulated. The asphere is designed according to a *theory of perfect aspheres* [16] with an NA of 0.8 and a working distance of 43 μm. The asphere is sampled in a 64^3 grid with $dx=dy=dz=0.6875$ μm. The asphere has a refractive index of 2 and the surrounding volume has a refractive index of vacuum.

The exact field distribution at the focus can be derived from vectorial Debye theory. Figure 3 shows the distribution of the E_x-, E_y-, and E_z-components of the vector field from vectorial Debye theory. The comparison of Fig. 3 with the results from the VWPM in Fig. 4 shows that the basic features are reproduced. The simulated focal spot is very close to the design focus position. The amplitudes show a slight deviation. Figure 5 shows a xz-plot of the TE-electric field distribution. The asphere in this case had a radius of 22 μm, a NA of 0.8 and a refractive index of $n=1.5$. The surrounding refractive index was 1, and sampling is $N_x=N_y=N_z=64$. The figure shows a diffraction-limited, unaberrated spot, as is to be expected from a perfect focusing lens. Also the focus location agrees perfectly with ray tracing. As reference, we also tried the

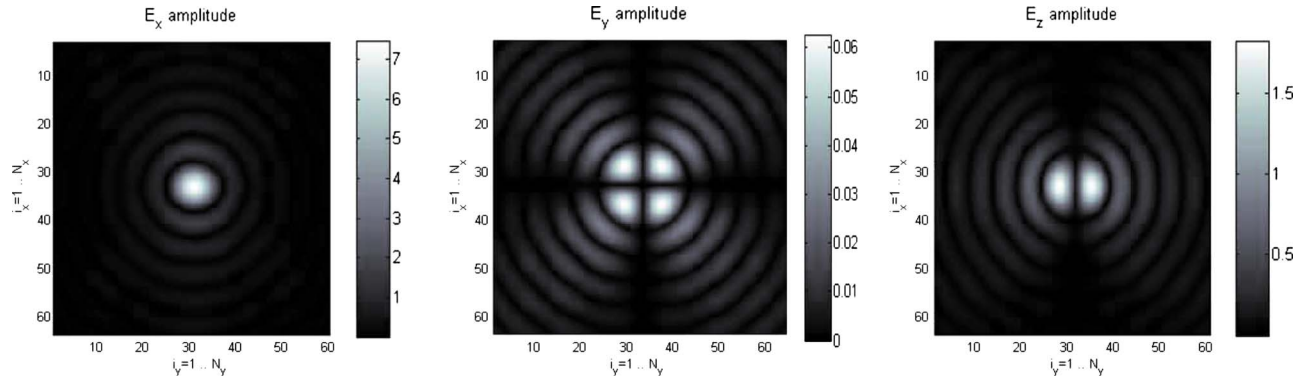

Fig. 3. (Color online) Amplitudes E_x (left), E_y (middle), and E_z (right) of the vector field at focal distance (vectorial Debye theory).

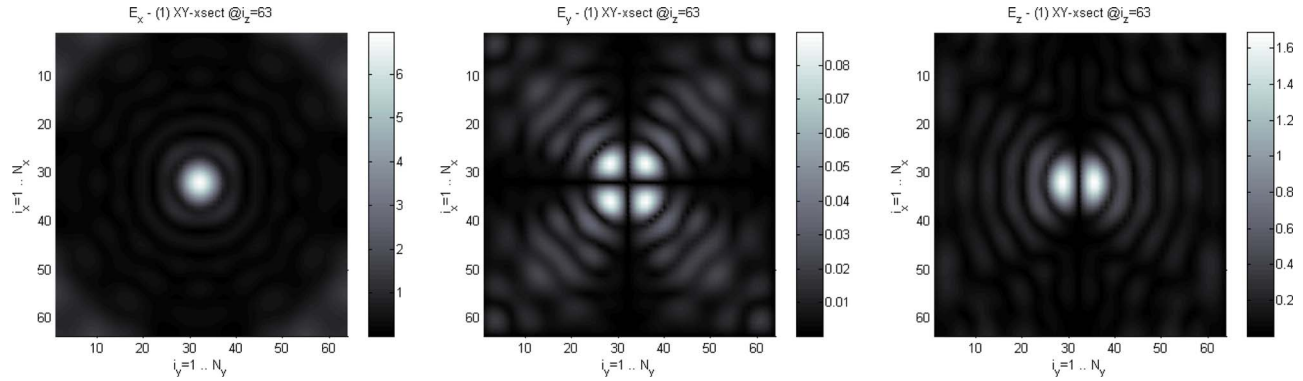

Fig. 4. (Color online) Amplitudes E_x (left), E_y (middle), and E_z (right) of the vector field at focal distance (VWPM).

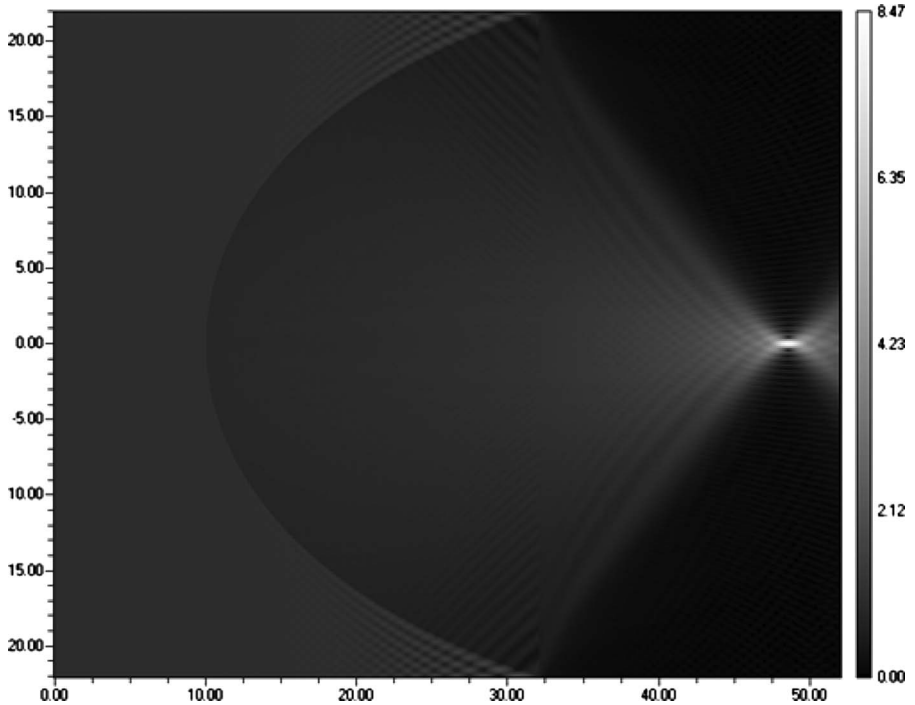

Fig. 5. Simulation of a perfect asphere with the VWPM. The figure shows the amplitude of the E_y-component of a TE-polarized plane wave that propagates from left to right through a perfect asphere.

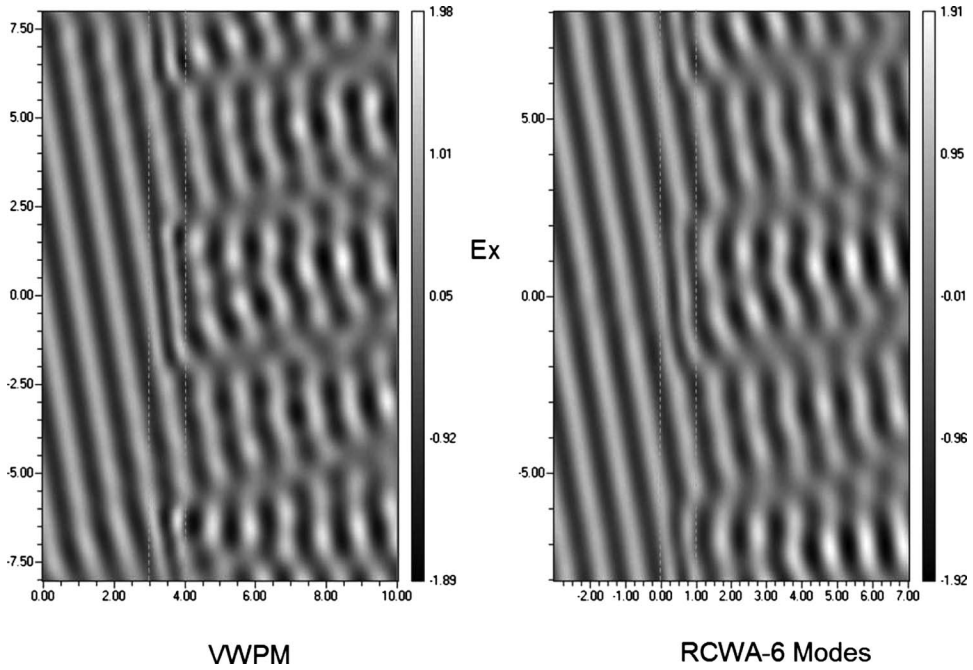

Fig. 6. Amplitude of the E_x-component of the vector field in the xz-plane simulated with RCWA (right) and the VWPM (left) for oblique incidence.

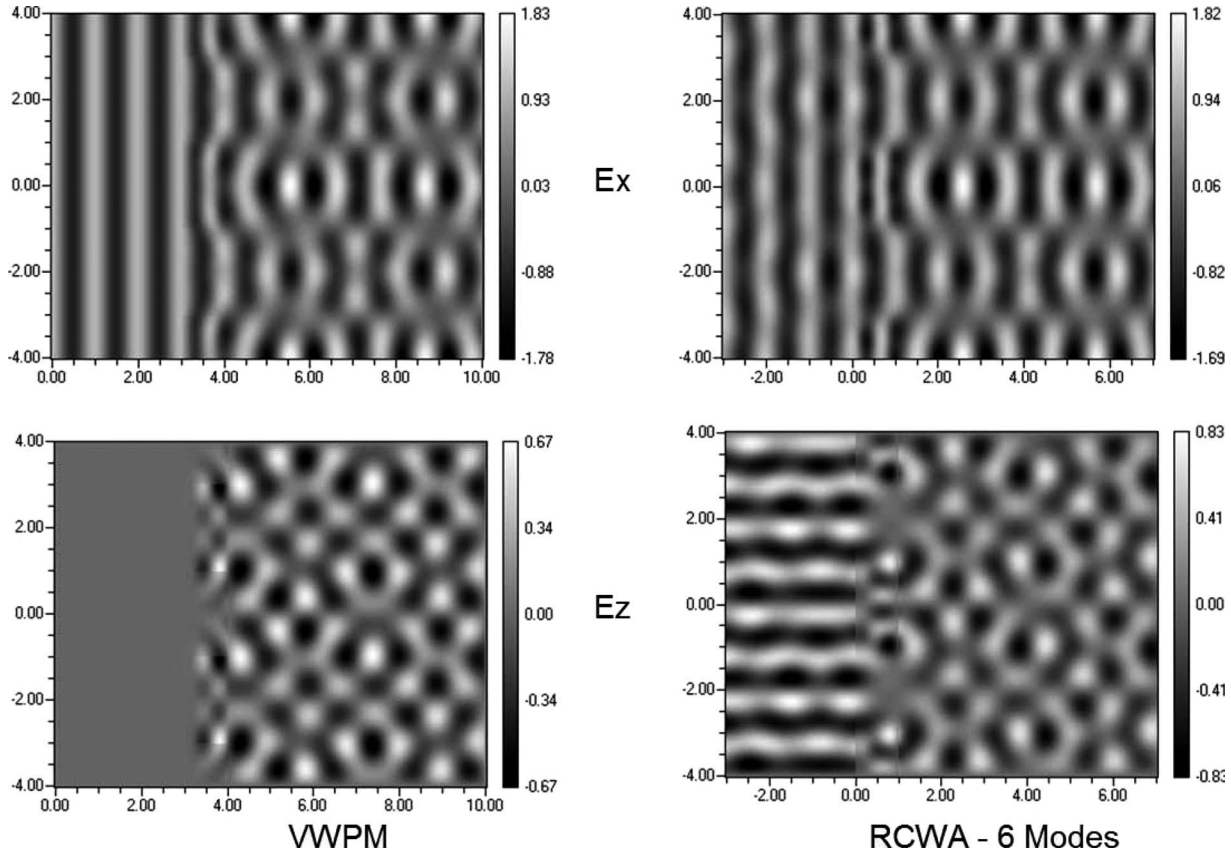

Fig. 7. Amplitude of the E_x (upper row) and E_z-component (lower row) of the vector field in the xz-plane simulated with RCWA (right) and the VWPM (left) for perpendicular incidence.

VBPM, results of which are not shown here. It showed a longitudinal shift of the focus and a significant spherical aberration.

9. THREE-DIMENSIONAL SIMULATION OF A TWO-DIMENSIONAL GRATING

A third scenario is a high frequency grating defined by periods p_x, p_y and widths w_x, w_y in the x- and y-axes. The widths determine the duty cycle of the grating. The height of the grating is h. The refractive index of the grating is $n_g=1.5$ and the surrounding refractive index is $n=1$ (i.e., vacuum). The sampling is $dx=dy=dz=0.125$ μm. The parameters of the gratings are $p_x=p_y=8\lambda$, $w_x=w_y=4\lambda$, and $h=1\lambda$ for the simulation shown in Fig. 6 and $p_x=p_y=4\lambda$, $w_x=w_y=2\lambda$, and $h=1\lambda$ for the simulation in Fig. 7. The incident plane wave has a wavelength of $\lambda=1$ μm and *TM* polarization for both examples. The angle of incidence is 15° in Fig. 6 and 0° in Fig. 7. The propagated wave shows a well-defined distribution of the field amplitude that is determined by the grating dimensions.

The vector components of the electric field calculated by the VWPM are compared to the results of the two-dimensional RCWA. For the RCWA, six modes have been used, while the VWPM effectively uses 256 modes. Both figures show remarkable agreement. The differences are significant only for the indicent region before the grating, which is clear since the VWPM does not consider reflections.

10. CONCLUSION

The VWPM is an efficient tool to calculate the propagation of a vector wave through an arbitrary three-dimensional system. TE and TM components of the electric field are transformed according to the Fresnel coefficients of amplitude, and the continuity of the field is preserved in three dimensions utilizing a linear approximation of the transversal components and the vector geometry of plane waves at a boundary. The simulations show that the VWPM is accurate for non-paraxial propagation. The computational effort for the VWPM is higher than that for the BPM but also significantly lower than that of the three-dimensional RCWA. This makes the VWPM competitive in terms of runtime and further extends its applicability. It is therefore perfectly positioned between rigorous methods and the split step propagation scheme, and the results show remarkable agreement with rigorous methods in the near field and the transmitted region. The wave propagation scheme furthermore provides efficient ways of parallelization to reduce runtime. In homogeneous media, the VWPM agrees perfectly with the vectorial version of the PWD.

REFERENCES

1. K.-H. Brenner and W. Singer, "Light propagation through microlens: a new simulation method," in Appl. Opt. **32**, 4984–4988 (1993).
2. M. Feit and J. Fleck, "Light propagation in graded index fibers," Appl. Opt. **24**, 3390–3998 (1978).
3. G. R. Hadley, "Wide-Angle beam propagation method using Padé approximant operators," Opt. Lett. **17**, 1426–1428 (1992).
4. C. Ma and E. Van Keuren, "A three-dimensional wide-angle BPM for optical waveguide structures," J. Lightwave Technol. **27**, 2595–2604 (2009).
5. P. Lee and E. Vogoes, "Three-dimensional semi vectorial wide-angle beam propagation method," J. Lightwave Technol. **12**, 215–225 (1994).
6. T. Anada, T. Hokazono, T. Hiraoka, J. Hsu, T. Benson, and P. Sewell, "Very-wide-angle beam propagation methods for integraded optical circuits.," IEICE Trans. Electron. **E82-C**, 1154–1158 (1999).
7. J. Yamauchi, Y. Nito, and H. Nakano, "A modified semivectorial beam propagation method retaining the longitudinal field component," in *Integrated Photonics and Nanophotonics Research and Applications (IPNRA)*, (Optical Society of America, 2008), paper IWB5.
8. P. Liu and B. J. Li, "Semivectorial beam-propagation method for analyzing polarized modes of rib waveguide.," IEEE J. Quantum Electron **28**, 778–782 (1992).
9. J. Wanguemert-Perez and I. Molina-Fernandez, "A novel Fourier based 3D full-vectorial beam propagation method,"Opt. Quantum Electron. **36**, 285–301(2004),
10. Y. Tsuji, M. Koshiba, and N. Takimoto, "Finite element beam propagation method for anisotropic optical waveguides.," J. Lightwave Technol. **17**, 723–828(1999).
11. M. Stern, "Semivectorial polarized finite difference method for optical waveguides with arbitrary index profiles," IEEE Proc. Part J, Opto-Electron. **132**, 56–63 (1985).
12. H. Pinheiro, A. Barbero, and H. Hernandez-Figueroa, "Full-vectorial FE-BPM approach for the analysis of anisotropic medium with off-diagonal permittivity terms," Microwave Opt. Technol. Lett. V. **25**, 12–14(2000).
13. S. Obayya and B. Rahman, "New vectorial numerically efficient propagation algorithm based on the finite element method," J. Lightwave Technol. **18**, 409–415 (2000).
14. P. Sewell, J. Wykes, A. Vukovic, D. W. P. Thomas, T. M. Benson, and C. Christopoulos, "Multigrid interface in computational electromagnetics," Electron. Lett. **40**, 162–163(2004).
15. http://www.lighttrans.com.
16. P. Török and P. Varga, "Electromagnetic diffraction of light focused through a planar interface between materials of mismatched refractive indices: an integral representation," J. Opt. Soc. Am. A **12**, 325–332 (1995).
17. H. Scheffers, *Vereinfachte Ableitung der Formeln für die Fraunhoferschen Beugungserscheinungen* (Physikalisch-Technische Reichsanstalt, 1942).
18. S. Ziolkowski and K.-H. Brenner, "Vectorial analysis and optimisation of ideal focusing lenses," in*European Optical Society Topical Meeting on Advanced Optical Imaging Techniques*, June 29–July 1, 2005, London (EOS, 2005), pp. 91–92.